**RESEARCH ARTICLE**

# Dissolvable Carboxymethylcellulose Microneedles for Noninvasive and Rapid Administration of Diclofenac Sodium

*Ana C. Q. Silva, Bárbara Pereira, Nicole S. Lameirinhas, Paulo C. Costa, Isabel F. Almeida, Patrícia Dias-Pereira, Inês Correia-Sá, Helena Oliveira, Armando J. D. Silvestre, Carla Vilela, and Carmen S. R. Freire\**

The aim of this study is to prepare dissolvable biopolymeric microneedle (MN) patches composed solely of sodium carboxymethylcellulose (CMC), a water-soluble cellulose derivative with good film-forming ability, by micromolding technology for the transdermal delivery of diclofenac sodium salt (DCF). The MNs with ≈456 µm in height displayed adequate morphology, thermal stability up to 200 °C, and the required mechanical strength for skin insertion (>0.15 N needle$^{-1}$). Experiments in ex vivo abdominal human skin demonstrate the insertion capability of the CMC_DCF MNs up to 401 µm in depth. The dissolution of the patches in saline buffer results in a maximum cumulative release of 98% of diclofenac after 40 min, and insertion in a skin simulant reveals that all MNs completely dissolve within 10 min. Moreover, the MN patches are noncytotoxic toward human keratinocytes. These results suggest that the MN patches produced with CMC are promising biopolymeric systems for the rapid administration of DCF in a minimally invasive manner.

## 1. Introduction

Acute (e.g., migraine and minor musculoskeletal injuries) and chronic (e.g., osteoarthritis) pain has a considerable impact on the welfare of patients and is routinely treated with pain-reliever medications.[1,2] Nonsteroidal anti-inflammatory drugs (NSAIDs), such as ibuprofen, naproxen, and diclofenac sodium salt (DCF), are over-the-counter medicines recommended as the first step in pain management due to their analgesic and anti-inflammatory effects, provided by the nonselective inhibition of regulatory cyclooxygenase enzymes (COX-1 and COX-2).[3,4] While most forms are nearly entirely absorbed after enteral (e.g., oral) administration, the effect of first-pass metabolism can considerably diminish

A. C. Q. Silva, B. Pereira, N. S. Lameirinhas, A. J. D. Silvestre, C. Vilela, C. S. R. Freire
CICECO–Aveiro Institute of Materials and Department of Chemistry
University of Aveiro
Aveiro 3810-193, Portugal
E-mail: cfreire@ua.pt
P. C. Costa, I. F. Almeida
UCIBIO–Applied Molecular Biosciences Unit
MedTech–Laboratory of Pharmaceutical Technology & Associate Laboratory i4HB–Institute for Health and Bioeconomy
Faculty of Pharmacy
University of Porto
Porto 4050-313, Portugal

P. Dias-Pereira
Institute of Biomedical Sciences Abel Salazar
ICBAS-UPorto
University of Porto
Porto 4050-313, Portugal
I. Correia-Sá
Department of Plastic
Aesthetic
Reconstructive and Aesthetic Surgery
Centro Hospitalar de S. João
Porto 4200-319, Portugal
H. Oliveira
Department of Biology & CESAM
University of Aveiro
Aveiro 3810-193, Portugal

**ADVANCED
SCIENCE NEWS**

www.advancedsciencenews.com

[M]acro-
molecular
Bioscience

www.mbs-journal.de

the bioavailability of these drugs. Moreover, owing to the nonselective inhibition of the COX enzymes, long-term systemic use may result in countless side effects, including cardiovascular, gastrointestinal, renal, and hepatic complications.[5,6] Another popular method of administration is via intravenous or intramuscular injection of the drug, which is equally challenging due to its intrusive nature, causing painful experiences that directly impact patient compliance, as well as the requirement of professional administration.[2]

As such, one of the main targets for NSAIDs administration in the management of musculoskeletal disorders is dermal application, as the localized administration of drugs is convenient for self-medication and can provide the therapeutic benefits of the active ingredients while reducing adverse systemic effects.[7] Several NSAID cutaneous formulations are already available on the market, including patches (Flector), solutions (Pennsaid), and gels (Voltaren, Solaraze).[8,9] These topical formulations are comprised of diclofenac salts, mainly of diclofenac sodium, as these drugs are highlighted as the most effective among the NSAIDs for pain management, even for the treatment of chronic conditions.[10,11] Some trials demonstrate that the dermal application of diclofenac shows equivalent analgesic action with a lower incidence of systemic adverse effects compared to oral intake of the same active principle.[12] Nonetheless, the barrier effect provided by the epidermis's outermost layer, the *stratum corneum*, is known to restrict the passive diffusion of active molecules through the skin, reducing their therapeutic effect.[7] Thus, there is a practical demand for transdermal delivery devices that can promote drug permeation across the skin while bypassing the physical barrier imposed by the *stratum corneum*.

Microneedles (MNs) are systems composed of an array of needle-like projections ranging in length from 25 to 2000 μm, capable of physically disrupting the *stratum corneum* and creating microconducts that allow molecules to pass through the skin in a painless, minimally invasive, and self-administrable manner, increasing patient compliance.[13] The US Food and Drug Administration (FDA) has already approved numerous products, including solid MNs for beauty skin treatments (Dermaroller and LiteClear), hollow MNs for vaccination (Soluvia), and dissolvable MNs for drug delivery (MicroHyala, Vaxmat, Drugmat).[14,15]

Dissolvable MNs manufactured with biopolymers (e.g., pullulan,[16] chitosan,[17] hyaluronic acid[18]) are particularly appealing in this situation as they are intrinsically biocompatible and sustainable. These MNs promptly dissolve when in contact with the interstitial fluid, releasing the active substances incorporated in their matrix.[7,13] Carboxymethylcellulose (CMC) is a nontoxic, water-soluble, film-forming cellulose derivative ordinarily employed in drug development[19,20] and, attending to its properties, has been fairly exploited for the fabrication of MNs for the delivery of vaccines, hormones, and other molecules, either exclusively[21–24] or in combination with other materials, like poly(vinylpyrrolidone),[25] layered double hydroxides,[26] and gelatin.[27]

Pretreatments with solid MNs are known to enhance the permeation of NSAID-based formulations across the skin by first disrupting the *stratum corneum* and creating micropores in the skin that enable a more efficient passage of the drug load subsequently applied.[28–30] Nonetheless, the design of dissolvable MNs that can simultaneously disrupt the *stratum corneum*

and deliver the bioactive compounds would be of great interest for a single-step transdermal administration of these widely used drugs. The design of such systems is scarcely reported in the literature, with knowledge of only two studies thus far dealing with the fabrication of dissolvable MNs for the administration of NSAIDs, namely, poly(methylvinyl ether/maleic acid) MNs for the delivery of ibuprofen[31] and hyaluronic acid/dextran/poly(vinylpyrrolidone)-layered MNs incorporating DCF and tacrolimus.[32] Nevertheless, to the best of our knowledge, there are no reports on dissolvable MNs composed of a single biopolymeric matrix component with the required properties for delivering such drugs.

In this vein, in the present study, we investigated the fabrication and characterization of dissolvable carboxymethylcellulose-based MNs for the noninvasive administration of DCF, envisioning quick pain relief. The MNs were produced via a simple micromolding approach and evaluated in terms of morphology, thermal stability, mechanical properties, skin penetration capability, and potential for DCF delivery. Moreover, the biocompatibility of the MN patches toward human epidermal keratinocytes (HaCaT cells) was assessed to infer the safety of these systems for skin drug administration applications.
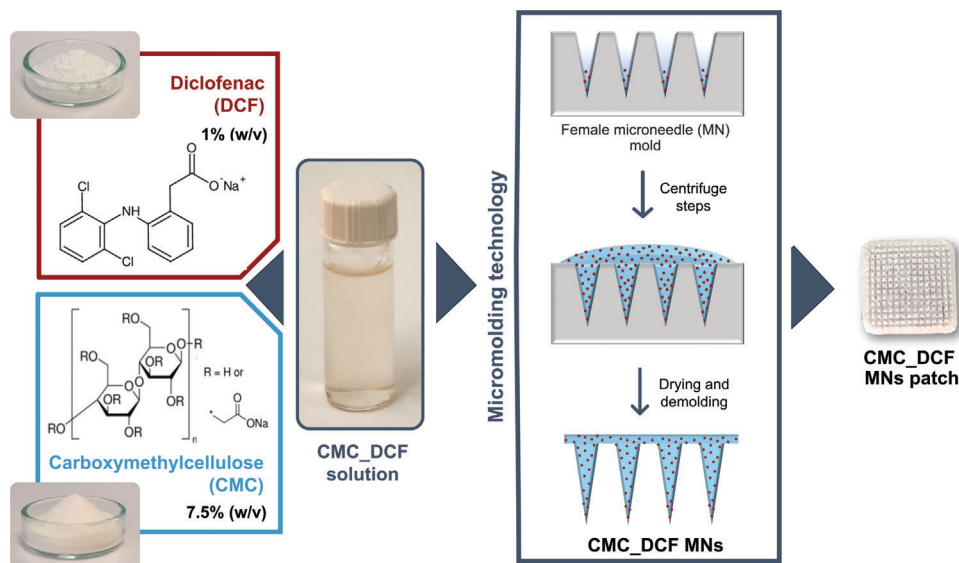
## 2. Results and Discussion

Pyramidal-shaped MN patches comprised of CMC and a NSAID, viz. diclofenac, were fabricated via the simple and affordable casting of aqueous solutions of CMC and DCF using female master molds (**Figure 1**). This cellulose derivative was chosen for its high water solubility and biocompatibility,[19] enabling the formulation of dissolvable MNs to deliver therapeutic drugs through the skin, resorting to a single polysaccharide matrix component. A CMC concentration of 7.5% w/v was selected due to the compromise between the viscosity of the solution and the integrity of the MN arrays obtained. DCF was used in a 1.0% w/v concentration, based on equivalent contents of commercial formulations.[33,34] The prepared CMC-based MN patches (viz. CMC and CMC_DCF MNs) were characterized in terms of morphology, mechanical performance, skin penetration ability, and thermal stability. In addition, the insertion capacity of the DCF-loaded MN systems was further evaluated in ex vivo abdominal human skin samples. Finally, the dissolution and release of diclofenac from the patches were assessed, as well as their biocompatibility toward human keratinocytes.

### 2.1. Characterization of the CMC and CMC_DCF MN Patches

#### 2.1.1. Morphology

As it can be observed in the optical micrographs displayed in **Figure 2**, the shape of the master mold was successfully replicated in both CMC and CMC_DCF MN patches, with evenly spaced pyramidal MN projections across the arrays. The coloration of the CMC arrays was off-white and slightly transparent, which is consistent with the common appearance of CMC-based films.[35] The CMC_DCF arrays exhibited a similar off-white color, displaying iridescence upon visual inspection due to the inclusion of the

**ADVANCED**
**SCIENCE NEWS**

www.advancedsciencenews.com

Macro-
olecular
Bioscience

www.mbs-journal.de

**Figure 1.** Schematic representation of the preparation of dissolvable CMC_DCF MNs via micromolding.
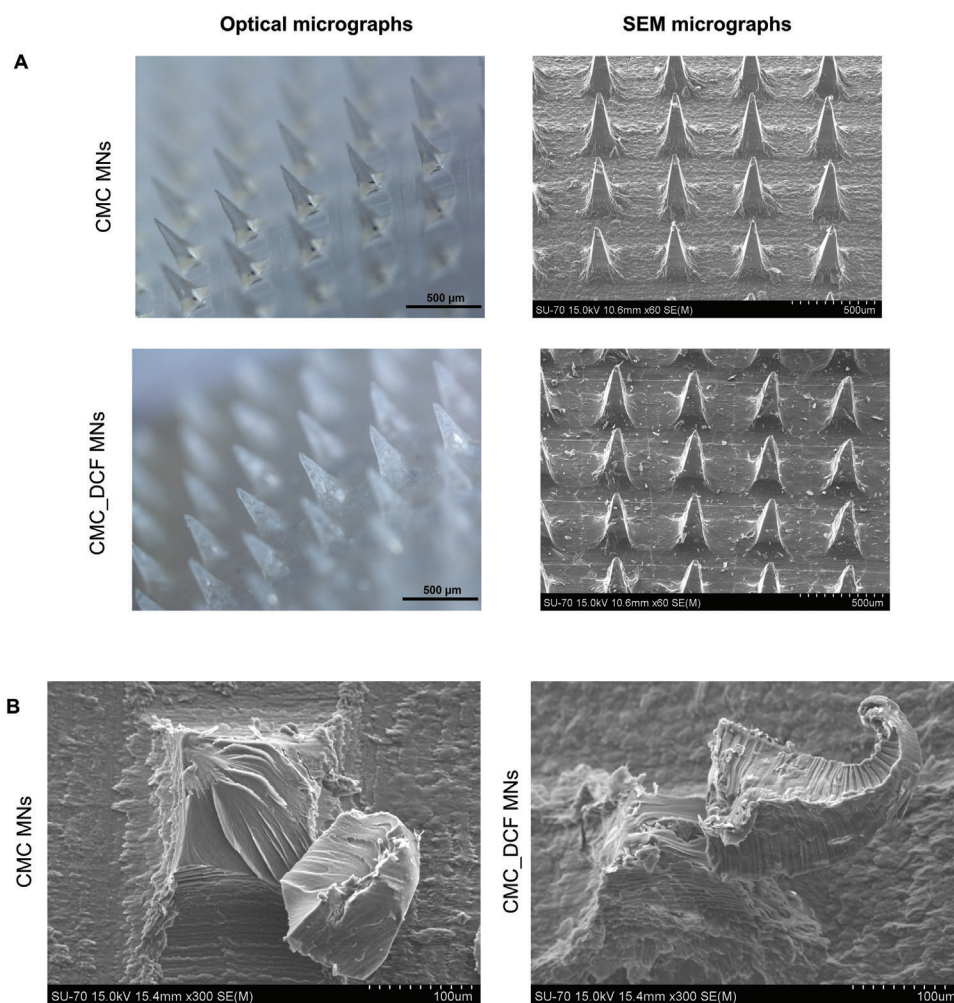


**Figure 2.** A) Optical and SEM micrographs of the CMC and CMC_DCF MNs (scale bars: 500 μm). B) SEM micrographs of the cross-section of the CMC and CMC_DCF MNs (scale bars: 100 μm).

# ADVANCED
## SCIENCE NEWS
www.advancedsciencenews.com

M acro-
olecular
Bioscience
www.mbs-journal.de

DCF drug in the polymeric matrix. Moreover, the MNs presented well-defined tips with an average diameter of 14 ± 3 μm for the CMC MNs and 15 ± 3 μm for the CMC_DCF MNs ($n = 35$), which is in line with the typical tip dimensions indicated for these systems (up to 25 μm).[15]

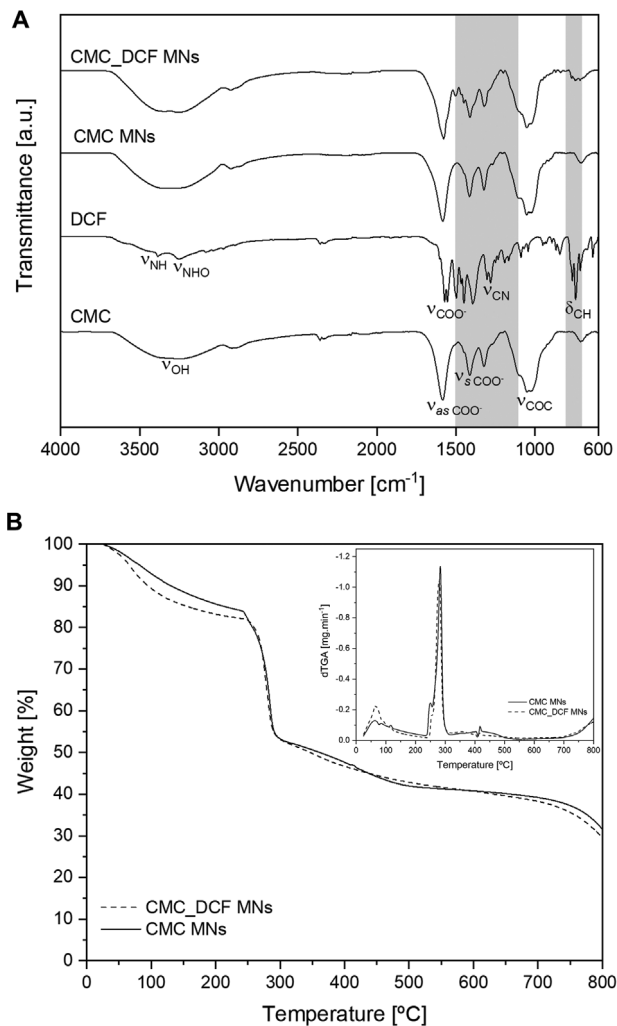In terms of dimensions, the pristine and diclofenac-loaded CMC MN patches display microprojections with 456 ± 27 and 456 ± 29 μm of height, respectively, and base width of 200 ± 1 μm for both systems. The reduction of the needle's height (≈17%), compared to the dimensions of the master mold, is generally credited to the evaporation of the solvent during the drying process, as previously described in similar works regarding the fabrication of MNs with CMC[22,26] and other biopolymers, namely, hyaluronic acid[18] and alginate.[22] In the case of the MNs prepared with CMC, height reduction values of 19%[22] and 24%[26] were observed for MNs prepared with CMC 5 wt% and CMC 5 wt% reinforced with layered double hydroxides, respectively. Therefore, a similar or lower decrease in needle height was obtained with these systems. Nevertheless, attending to the average thickness of each skin layer, the height values obtained for these MNs suggest their ability to disrupt the *stratum corneum* (10–20 μm), penetrate the viable epidermis (50–100 μm), and reach the dermis layer (1–3 mm) without stimulating nociceptors nor puncturing blood vessels.[13]

The scanning electron microscopy (SEM) micrographs of the MN arrays (Figure 2A) highlight the pyramidal shape of the MNs, as observed previously in the optical micrographs. Moreover, the surface (Figure 2A) and cross-section (Figure 2B) micrographs reveal that no bubbles or fissures were found in the body of the needles, which are fully filled with the polymer and DCF, highlighting the uniformity of the needle matrices in both the CMC and CMC_DCF samples.

### 2.1.2. Fourier Transform Infrared-Attenuated Total Reflection (FTIR-ATR) Spectroscopy

The FTIR-ATR spectra of the CMC and diclofenac-loaded CMC MNs, as well as of the CMC and DCF powders for comparison, are illustrated in **Figure 3**A. The IR spectrum of CMC depicts the main bands attributed to cellulosic substrates, namely, a broad band located at 3249 cm$^{-1}$, ascribed to the O–H stretching vibrations ($\nu_{OH}$), and a weaker signal at 2915 cm$^{-1}$, resultant from the stretching vibration of the C–H bonds ($\nu_{CH}$).[36,37] The absorption bands found in the 1200–970 cm$^{-1}$ range correspond to the stretching of the C–O ($\nu_{CO}$) bonds of the pyranoid ring and the C–O–C stretching ($\nu_{COC}$) of the glycosidic bonds.[36,37] The CMC spectrum also reveals the characteristic asymmetric and symmetric stretching vibrations of the carboxylate group ($\nu_{COO^-}$) at 1585 and 1413 cm$^{-1}$, respectively.[38] In the spectrum of DCF powder, distinctive absorption bands can also be recognized, namely, at 3385 cm$^{-1}$ (–NH stretching of the secondary amine, $\nu_{NH}$), 3250 cm$^{-1}$ (NH–O stretching, $\nu_{NHO}$), 1572 cm$^{-1}$ (–COO stretching, $\nu_{COO^-}$), 1350–1250 cm$^{-1}$ (C–N stretching, $\nu_{CN}$), and 745–730 cm$^{-1}$ (C–H out-of-plane bending, di- and tri-substituted rings, $\delta_{CH}$).[39,40]

The IR spectrum of the CMC MN patches is identical to that of CMC powder because it is the unique component of this system, and no structural modifications of the polymer were expected to occur during the dissolution and casting of the CMC solution. The spectrum of CMC_DCF MNs follows the general tracing pattern of CMC, particularly in the 1200–970 cm$^{-1}$ range, given that the cellulosic derivative is the major component of these arrays (Figure 3A). Nevertheless, the appearance of a slight shoulder at 3362 cm$^{-1}$, resultant of the –NH stretching vibration, and discrete bands in the 1500–1100 and 800–700 cm$^{-1}$ ranges confirm the presence of DCF in the MN array (Figure 3A). Moreover, no peak displacement was perceived, indicating that no strong interactions between the drug and the polymer were established.

### 2.1.3. Thermogravimetric Analysis (TGA)

The thermal stability of the CMC and CMC_DCF MN patches was evaluated under an inert atmosphere (N$_2$) by TGA (Figure 3B). Attending to the strong hydrophilic nature of CMC, an initial weight loss of ≈7.1–10.6 wt% is observed for temperatures below 100 °C for both samples and can be attributed to
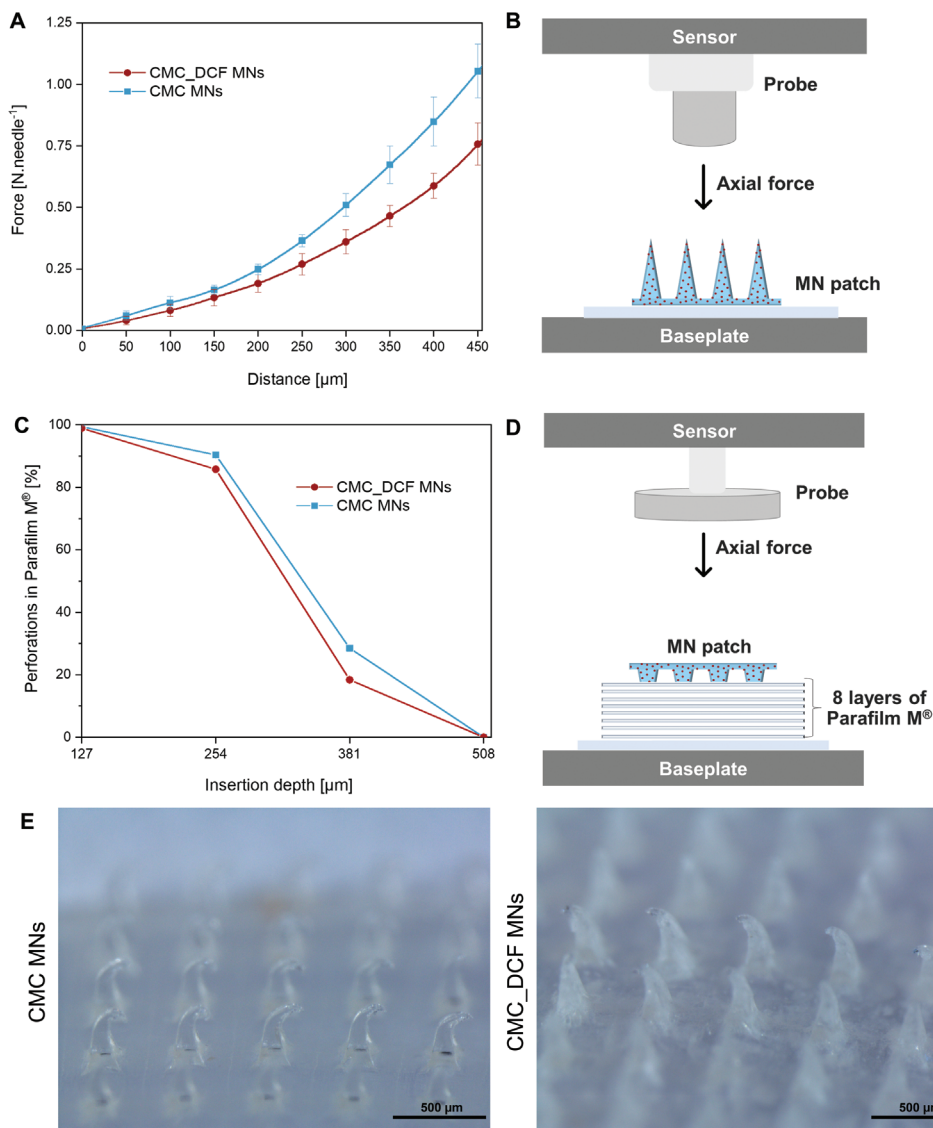


**Figure 3.** A) FTIR-ATR spectra of the CMC and DCF powders and the pristine and drug-loaded CMC MNs. B) Thermograms and respective derivatives (inset graphic) of the MN patches under an inert atmosphere.

**ADVANCED
SCIENCE NEWS**

www.advancedsciencenews.com

[M] **acro-
olecular**
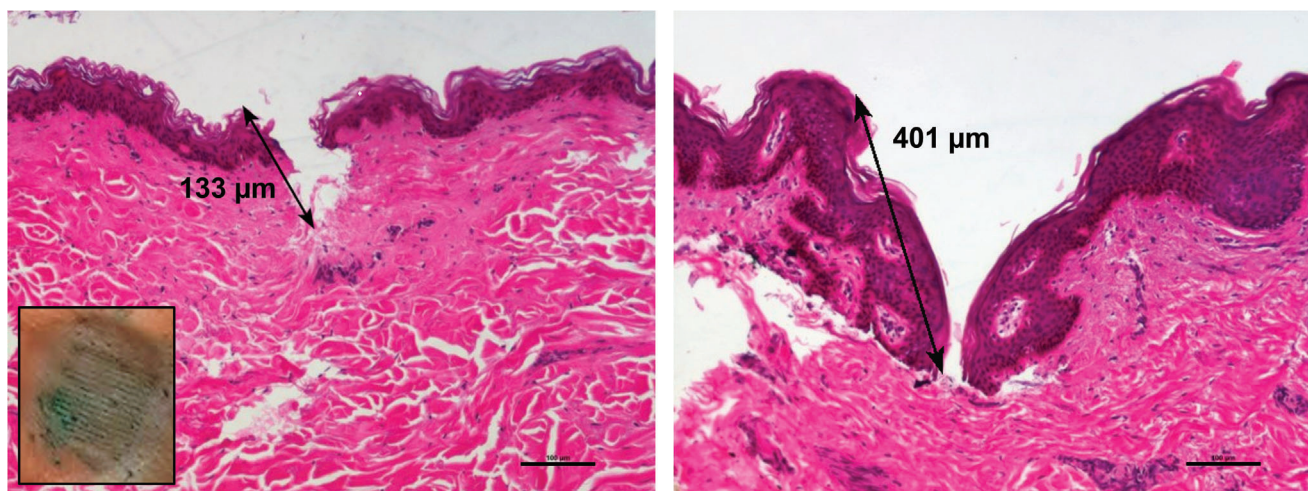**Bioscience**

www.mbs-journal.de

**Figure 4.** A) Plot of the force versus displacement curves of the CMC MNs with and without diclofenac (the values are the mean of nine replicates, the errors bars correspond to the standard deviations, and the lines are for visual guidance only) and B) Scheme of the mechanical axial test. C) Graphical representation of the insertion ability of the MNs in a polymeric skin model Parafilm M (error bars are smaller than the data point, and the lines are for visual guidance only) and D) Scheme of the set-up for the test. E) Optical micrographs of the CMC and CMC_DCF MNs after insertion in the Parafilm M model (scale bars: 500 μm).

moisture loss.[41] Apart from the dehydration of the sample, the thermograms of the MNs display a single weight-loss degradation step, with a maximum degradation temperature ($T_{dmax}$) of 284 and 280 °C, and a final residue of 31.6 wt% and 29.7%, for the CMC MNs and CMC_DCF MNs, correspondingly. This behavior is typical of the cellulosic derivative[36,42] and represents the decarboxylation and pyrolysis of the cellulosic skeleton. Moreover, the degradation profile of both MN samples is similar due to the low quantity of DCF incorporated in the MNs, causing only a slight decrease (≈4 °C) in the $T_{dmax}$. As a result, the MN patches are thermally stable up to 200 °C, allowing the use of conventional sterilization processes that demand high temperatures, such as autoclaving (≈121 °C), in the preparation of drug delivery systems.

*2.1.4. Mechanical Evaluation and Preliminary Insertion Studies in Parafilm M*

The assessment of the mechanical properties of MNs plays a critical part in their development, as the MNs arrays are subjected to stresses upon skin insertion that could lead to failure of the system. The mechanical behavior of the MN patches was accessed by their force versus displacement profiles, resultant of the application of an axial compression force against the MNs placed in a flat and rigid support (**Figure 4**A,B). The obtained plots display no discontinuities and a gradual increase in the force per needle value, indicating that the needles do not break but instead suffer deformation upon applying the force load. This behavior is typical of polymeric MNs (i.e., poly(lactic acid), CMC) with a

**ADVANCED
SCIENCE NEWS**
www.advancedsciencenews.com

{M}acro-
olecular
**Bioscience**
www.mbs-journal.de

**Figure 5.** Digital photograph of the perforation marks on excised human skin after CMC_DCF MNs insertion (inset) and histological sections of the skin specimens (scale bars: 100 µm).
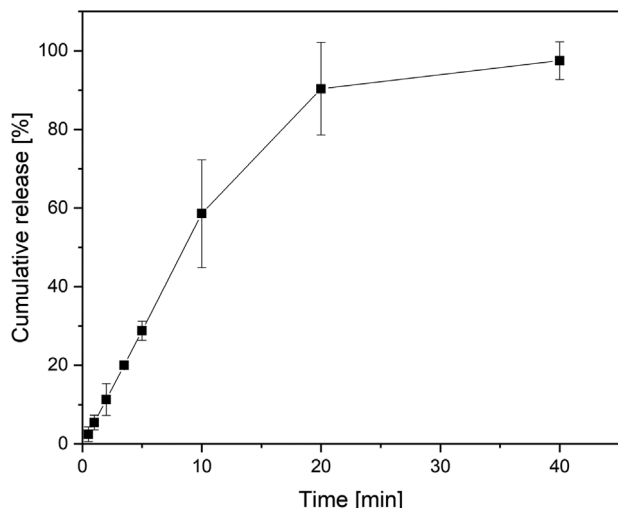
pyramidal shape, in contrast to conical ones, which possess a failure point.[21] At displacements of 200 and 450 µm, the CMC patch can withstand a force load of 0.25 and 1.05 N needle$^{-1}$, respectively. The incorporation of the drug in the patch causes a decrease to 0.19 and 0.75 N needle$^{-1}$ for the same displacement values. In any case, the MNs can support the force values reported in the literature required for disruption of the top skin layer (0.058 N) and insertion without breakage (0.15 N needle$^{-1}$), confirming that they are suitable for human skin penetration.[13,43] Indeed, at the highest displacement tested (450 µm), both MN patches surpass the failure point previously observed for conical MNs produced with pristine CMC at 10% (0.513 N needle$^{-1}$)[24] and 14% w/v (0.65 N needle$^{-1}$).[23] In the case of pyramidal MNs produced with CMC, the force load reported in a previous study at 200 µm displacement was higher (0.6 N needle$^{-1}$).[21] However, the CMC concentration (27 wt%) and the MNs height (600 µm) were superior, compared to the MNs prepared in the present study. Similarly, MNs prepared with other natural polymers displayed forces in a close range (0.2–0.4 N needle$^{-1}$ for 10 wt% chitosan[17] and 0.17–0.30 N needle$^{-1}$ for 5% w/v hyaluronic acid[18]), at the same displacement value. Moreover, the MNs produced in this study using a single matrix constituent, viz. CMC, reveal a higher force value than the previously reported dissolvable layered MNs with DCF (0.6 N needle$^{-1}$),[32] fabricated using different blends of polymers and nicotinamide in the interlayer to enhance the mechanical strength.

To further investigate the ability of the MNs for skin insertion, the patches were placed on the top of the eight Parafilm M layers and subjected to an axial force of 40 N for 30 s (Figure 4C,D). The MNs could penetrate the film and reach the third layer, corresponding to a thickness of 381 µm. Practically all the projections of the CMC and CMC_DCF MNs pierced the first layer of the film (99%, for both cases), and 90% and 86% penetrated the second layer, respectively. However, only a small fraction of the MN's projections could puncture the third layer, with values of 29% for the CMC MNs and 18% for the CMC_DCF MNs. This profile is similar to those reported for Gantrez S-97[44] and pullulan[16,45] MNs,

using the same methodology. None of the MN patches reached the fourth layer of the Parafilm M model (508 µm depth), which was anticipated considering the height of the needles. Moreover, with respect to the penetration depths of both MNs systems, the MNs are expected to avoid contact with blood capillaries and peripheral nerves that lie predominantly in the dermal layer.[13] The retrieved patches were likewise examined using optical microscopy to verify the integrity of the MNs following insertion in the Parafilm M model (Figure 4E). As expected, given their pyramidal geometry,[21] the needles do not break after insertion but rather suffer a slight deflection of the needle tips without causing damage to the needles' bodies. This assessment, once again, demonstrates their ability to withstand the required force for skin insertion without fracturing.

## 2.2. In Vitro Skin Insertion of DCF-Loaded MNs

Afterward, the feasibility of the patches for skin insertion was evaluated in ex vivo human skin. The MNs were inserted in excised human skin with a force of 40 N for 30 s, using the Texture Analyzer. After removing the CMC_DCF MN patches, staining with China ink disclosed the insertion marks of the MNs in the skin (**Figure 5**, inset). Histological analysis of the specimens revealed the formation of conducts in the skin with depths varying from 133 to 401 µm (Figure 5), corresponding to 29–88%, relative to the needle's height. The insertion percentages are analogous to published data regarding the insertion of sulforhodamine B-loaded CMC MNs[21] in cadaver pig skin (25–33%), and of CMC MNs reinforced with layered double hydroxides[26] in both cadaver pig skin (≈43%) and abdominal human skin ex vivo (≈39%). This value is also higher than the insertion capacity of dissolvable MNs composed of a mixture of polymers containing the DCF drug (≈50%, in Sprague–Dawley rat skin).[32] These results evidenced that the DCF-loaded CMC MN patches were able to penetrate the *stratum corneum* and the epidermis successfully, as predicted in the Parafilm M assay, creating microchannels that

**ADVANCED**
**SCIENCE NEWS**

www.advancedsciencenews.com

[M] **acro-**
**molecular**
Bioscience
www.mbs-journal.de

**Figure 6.** Cumulative dissolution profile of DCF from the drug-loaded CMC MN patches in phosphate buffer solution (the values are the mean of four replicates, the error bars correspond to the standard deviations, and the lines are for visual guidance only).

would allow the dissolution of the biopolymeric MNs and consequent release of DCF molecules therein enclosed, while minimizing the contact with the nerve fibers and blood vessels of the underlying dermal layer.

### 2.3. In Vitro Drug Release

The in vitro dissolution of diclofenac from the CMC_DCF MNs was first investigated in a phosphate buffer solution (PBS) to assess the delivery profile of these patches. As illustrated in **Figure 6**, an initial quick-release of DCF is observed, followed by a slower phase where the cumulative drug release attains the highest value. In detail, an initial cumulative release of 5% was achieved at 1 min, and about 29% of DCF was liberated from the MNs after 5 min. By the 10 min point, the system had already released more than half of its loaded drug content ($\approx$58%) and steadily reached the maximum cumulative release of 98% after 40 min. This dissolution pattern has been described in the release of this pharmaceutical agent from other polymeric systems, e.g., hyaluronic acid and bacterial nanocellulose patches[40] and Eudragit microspheres.[46]

Considering that research involving animal models poses ethical concerns and difficulties in the experiments due to the natural skin variability, a physical skin model (an agarose hydrogel) was chosen to carry out dissolution studies of the MNs.[47] Initially, the dissolution of the CMC_DCF MNs was visually appraised at different time points after the insertion of the patch in the agarose hydrogel (**Figure 7**A–F). The MN projections in the patch are still evident after 30 s but as small and evenly distributed white markings. The uptake of water from the skin simulant and disintegration of the polymeric matrix is witnessed after 1 min, with the fading of the white speckles in the patch corresponding to
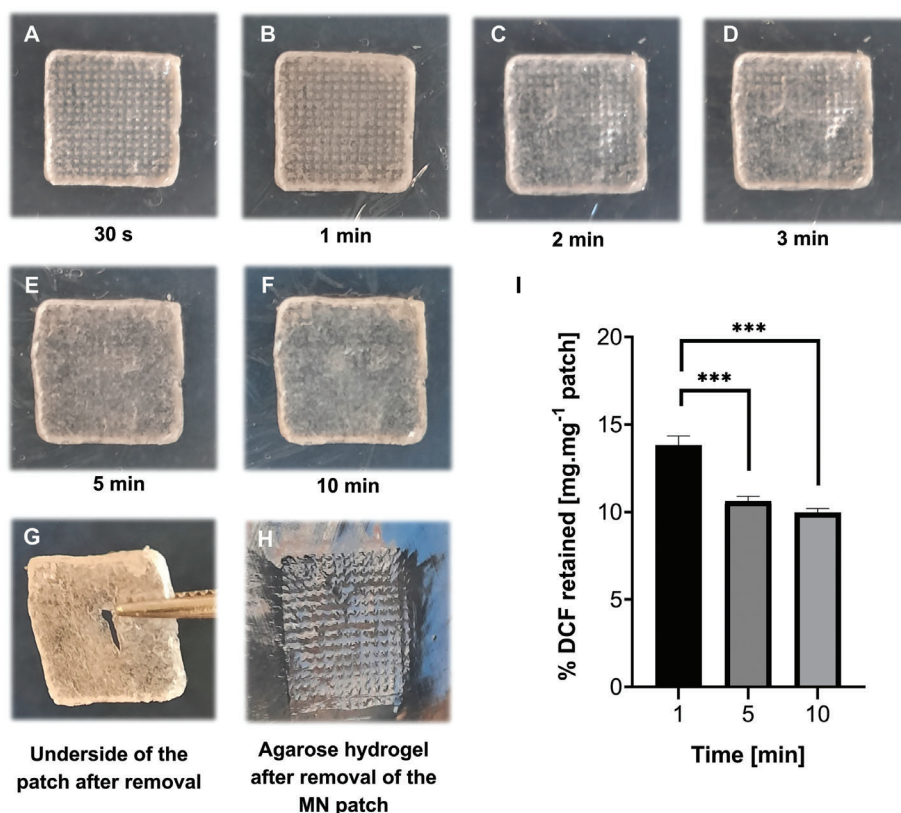


**Figure 7.** Digital photographs of A–F) the CMC_DCF MN inserted in an agarose skin model for different times, G) of the underside of the patch, and H) the agarose hydrogel upon removal of the patches. I) Graphical representation of the percentage of DCF retained in the MNs after 1, 5, and 10 min of insertion (*** denotes statistically significant differences, $p < 0.001$).

**2200323 (7 of 11)**

the pyramidal projections of the MNs. After 10 min, all MNs appeared to be fully dissolved, and the remnant of the MN patch was retrieved from the film's surface with tweezers (Figure 7G). Only the backing layer of the patch remained on top of the film, and the underside of the patch was free of needle-like projections, indicating that all MNs had been dissolved (Figure 7G). The puncture marks in the hydrogel after removing the patch illustrate the penetration of the MNs in the agarose medium (Figure 7H).

To further elucidate the drug release profile from the patches, CMC_DCF MNs were inserted in the skin model, retrieved after 1, 5, and 10 min, and the residual amount of DCF in the patches was quantified (Figure 7I). After only 1 min of insertion, the patches released about 85% of the DCF, as only 15% of DCF, relative to the initial mass of the patch, was determined on the retrieved patches. As expected, for longer insertion times, less amount of DCF was retained in the MNs (less than 10% for 10 min) since the insertion process enabled the MNs to come into contact with the water present in the agarose hydrogel, dissolving the polymeric matrix and releasing the pharmaceutical agent into the medium.

### 2.4. In Vitro Cytotoxicity Assay

The safety assessment is critical in the development of materials intended for biomedical applications.[48] In this vein, the cytotoxicity of both CMC and CMC_DCF MNs patches toward human keratinocytes was assessed using the 3-(4,5-dimethylthiazolyl-2)-2,5-diphenyltetrazolium bromide (MTT) assay. After 24 h of exposure to the MNs samples, the metabolic activity of the HaCaT cells was barely unaffected compared to the negative control (100% cell viability), with cell viabilities above 91 ± 4% and 88 ± 10% for the CMC and CMC_DCF MNs, respectively (**Figure 8**). Thus, these materials are considered noncytotoxic under the ISO 10993-5:2009(E) standard since a reduction of less than 30% in cell viability is detected. These findings were anticipated, given the biocompatible nature of the major component of the patches, viz. CMC.[19,20]

### 3. Conclusion

In this study, dissolvable CMC MNs loaded with diclofenac sodium were fabricated by micromolding. The incorporation of DCF in the CMC MN matrix was easily attained by the addition of the drug in the CMC solution before solvent casting. The obtained pyramidal MNs presented uniform morphology and size, and good mechanical and thermal properties. The DCF-loaded MNs could successfully pierce and disrupt the outermost layer of human skin, with insertion depths of 29–88% relative to the needle's height. The MN patches released ≈98% of the incorporated drug after 40 min of dissolution in PBS. Moreover, they were noncytotoxic toward HaCaT cells. These findings suggest that the ensuing MNs, comprised of a single biopolymeric matrix constituent, may be an attractive platform for the transdermal delivery of NSAIDs, like DCF, to conquer pain relief in a minimally invasive fashion.
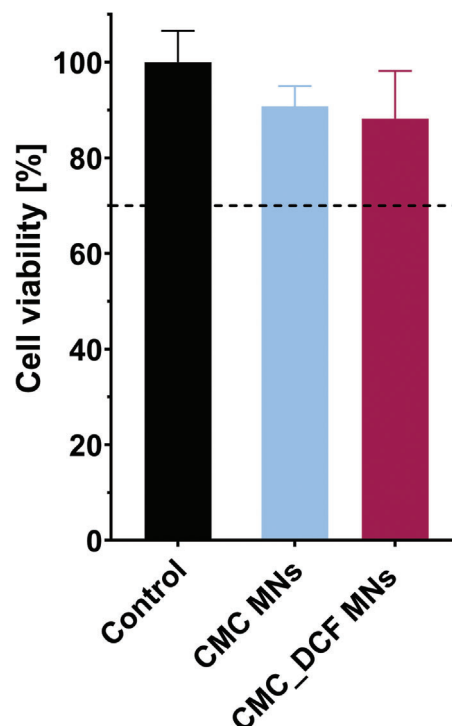


**Figure 8.** Cell viability [%] of the HaCaT cells after 24 h of exposure to the CMC and CMC_DCF MNs samples. The dashed line represents the threshold of cell viability for nontoxic materials, i.e., 70%.

### 4. Experimental Section

*Chemicals, Materials, and Cells*: Sodium carboxymethylcellulose salt (CMC, molecular weight (Mw) ≈ 250 000 g mol$^{-1}$, degree of substitution 1.2), diclofenac sodium salt (DCF, ≥98%), sodium phosphate dibasic (ACS reagent, anhydrous, ≥99.0%), potassium phosphate monobasic (ACS reagent, ≥99.0%), potassium chloride (BioXtra, ≥99.0%), dimethyl sulfoxide (DMSO, ReagentPlus, ≥ 99.5%), and ethylenediaminetetraacetic acid disodium salt dihydrate (EDTA, for molecular biology, 99.0–101.0% (titration)) were acquired from Sigma-Aldrich (St. Louis, MO, USA). Sodium chloride (ACS reagent, anhydrous, ≥99.5%) was obtained from Fluka (Sigma-Aldrich, Germany), and MTT (98%) was acquired from Alfa Aesar (Haverhill, Massachusetts, USA). Agarose basic (for molecular biology, gel point: 36.0 ± 1.5 °C) was purchased from Panreac (AppliChem GmbH, Darmstadt, Germany). Dulbecco's modified Eagle's medium (DMEM), fetal bovine serum (FBS), and trypsin/EDTA were acquired from PAN-Biotech GmbH (Aidenbach, Germany). PBS (pH 7.4), L-glutamine, and penicillin/streptomycin were purchased from Grisp, Lda. (Porto, Portugal). Fungizone was obtained from Gibco (Life Technologies, Carlsbad, CA, USA). Other chemicals and solvents were of laboratory grade and used as received. Ultrapure water (Type 1, 18.2 MΩ cm at 25 °C) was obtained using a Simplicity Water Purification System (Merck, Darmstadt, Germany). Nontumorigenic immortalized human keratinocytes (HaCaT cells) were acquired from Cell Lines Services (Eppelheim, Germany).

*Fabrication of the MN Patches*: Pyramidal MNs were prepared by micromolding using polydimethylsiloxane female molds (64 mm$^2$, 15 × 15 needles) with needle's height of 550 µm, base of 200 µm, and pitch of 500 µm (Micropoint Technologies Pte Ltd., Singapore). The appropriate CMC concentration was defined by producing MN arrays with 5, 7.5, and 10% w/v CMC aqueous solutions. Due to the high viscosity of the 10% solution, complete arrays could not be cast. Moreover, only the MNs prepared with the CMC solution of 7.5% w/v exhibited full needles with well-defined tips (data not shown). Given so, a CMC concentration of 7.5% w/v

ADVANCED
SCIENCE NEWS

www.advancedsciencenews.com

Macro-
molecular
Bioscience

www.mbs-journal.de

was selected for the MNs production. Briefly, the molds were progressively filled with the CMC solution at 50 °C and centrifuged at 6000 rpm for 5 min (Hettich Rotofix 32A) between each addition until the molds were entirely filled (≈160 mg). The molds were cast overnight at 28 °C in a ventilated oven to allow for solvent evaporation, and the CMC MNs were then gently peeled off from the molds and kept in a desiccator until further use. The preparation of the diclofenac-loaded MNs (CMC_DCF MNs) followed the same procedure, except that DCF (1.0% w/v) was incorporated into the CMC solution before the addition to the mold. To guarantee the complete dissolution of DCF in the CMC solution, DCF powder was added to ultra-pure water and dissolved before the addition of CMC.

*Morphological Characterization of the MN Patches*: Microscope images of both sets of MNs (CMC and CMC_DCF) were obtained with a stereomicroscope (Nikon SMZ18, Tokyo, Japan) coupled with an SRH Plan Apo 2 camera (Tokyo, Japan) and processed with NIS Elements Imaging Software. Five arrays of each sample were indiscriminately chosen to measure the needle's height ($n = 75$), base width ($n = 75$), and tip diameter ($n = 35$). The MN's surface and cross-section (fractured in liquid nitrogen) were also assessed using SEM micrographs obtained with a high voltage microscope (Hitachi SU 70, Tokyo, Japan) operated at 15 kV. Before analysis, samples were placed on an aluminum plate and coated with a carbon film (EMITECH K950, Laughton, UK).

*FTIR-ATR Spectroscopy*: FTIR-ATR spectra of the two components (CMC and DCF) and the fabricated MNs were recorded with a Perkin-Elmer FT-IR System Spectrum BX spectrophotometer (Perkin-Elmer Inc., MA, USA) equipped with a single horizontal Golden Gate ATR cell. Each spectrum was acquired over 32 scans, in the range of 600–4000 $cm^{-1}$, at a resolution of 4 $cm^{-1}$.

*TGA*: TGA of the MN patches was accomplished with a SETSYS Setaram TGA analyzer (SETARAM Instrumentation, Lyon, France) equipped with a platinum cell. The samples were heated from room temperature to 800 °C, at a constant rate of 10 °C $min^{-1}$, under an inert ($N_2$) atmosphere.

*Mechanical Characterization of the MN Patches*: The mechanical properties of the MN patches were evaluated through mechanical axial compression tests using a TA.XT2 Texture Analyzer (Stable Micro Systems Ltd., Haslemere, UK) equipped with a P/2 (2 mm diameter) stainless-steel probe.[16] The MN patches were fixed on a flat stainless-steel test station and subjected to a force perpendicular to the array's axis, applied at a constant speed of 0.01 mm $s^{-1}$ to mimic the force faced by the needles upon skin application. After the motion sensor met the needle's tip, the exerted force was measured as a function of needle displacement ($n = 9$).

*Preliminary Insertion Tests in a Film Model*: To investigate the penetration ability of the MN arrays, Parafilm M (Bemis Company Inc., Soignies, Belgium) was folded into eight layers (≈1 mm) to replicate the thickness of excised skin.[44] The MN patches ($n = 3$) were inserted into the folded film with a force of 40 N for 30 s, using the Texture Analyzer equipped with a P/6 (6 mm diameter) probe, and then removed to retrieve the punctured Parafilm M. Each layer of the film was inspected under an optical microscope (Olympus BX51, Olympus Corporation, Tokyo, Japan), and the resultant number of micropores per layer was counted to determine the insertion ratio and depth.[16] The retrieved MN patches were inspected using the stereomicroscope to evaluate the integrity of the samples after insertion in the Parafilm M model.

*In Vitro Skin Insertion*: The potential for skin insertion was further evaluated by inserting the CMC_DCF MNs in excised human abdominal skin tissue recovered from female donors subjected to an abdominoplasty procedure at Centro Hospitalar de São João–CHSJ (Porto, Portugal). The excised skin was pretreated and stored in a freezer at −20 °C until further use.[16] Before analysis, the skin was defrosted, sliced into circles with a biopsy punch (Ø = 25 mm), and sealed in a Petri dish for 1 h, on top of a cotton round embedded in PBS. Each circle was secured into a rigid support with hypodermic needles, and the MN arrays ($n = 3$) were pressed against the skin surface (30 s, 40 N) using the Texture Analyzer. After removing the MN patches, China ink was applied to the surface of the samples and then wiped to disclose the MN perforation sites. To prepare the specimens for histological examination, the skin samples were immersed in Bouin's solution, fixed in 10% formalin, dehydrated, and embedded in paraffin wax. A Rotary 3006 EM automated microtome was used to cut

serial 7 µm thick sections from each block, which were then stained with hematoxylin and eosin and inspected using a Nikon Eclipse E600 microscope. The study was conducted in accordance with the Declaration of Helsinki, and approved by the Ethics Committee of Centro Hospitalar S. João (Protocol 61-15, approved 13 May 2015).

*In Vitro Drug Release Study in PBS*: The release profile of DCF in a buffer solution was carried out by immersing CMC_DCF MN patches ($n = 4$) in a vial containing 10 mL of PBS (37 °C, 50 rpm). At predetermined time intervals, 1 mL of solution was withdrawn and replaced with the same volume of fresh, preheated buffer solution to maintain a constant volume in the vessel. The DCF content in each aliquot was determined by UV-vis spectroscopy at $\lambda = 276$ nm (Thermo Scientific Evolution 600, Thermo Fisher Scientific, Waltham MA, USA).[40] The DCF content at each time was calculated as a cumulative release percentage using Equation (1), where $C_n$ and $C_{n-1}$ are the DCF concentrations at times $n$ and $n-1$

$$C_{cumulative} = C_n + [(1 \times C_{n-1})/10] \tag{1}$$

The concentrations were calculated using a linear calibration curve ($y = 14.988 x - 0.001$; $R^2 = 0.9998$) obtained by measuring the absorbance of DCF solutions (0.001–0.06 mg $mL^{-1}$) at the same wavelength. The amount of diclofenac per patch (1.57 mg) was determined via the density value of the CMC_DCF solution at the working temperature ($\rho = 1.019$ g $cm^{-3}$), acquired with an automated SVM3000 Anton Paar rotational Stabinger viscometer–densimeter equipment.[49]

*Dissolution Tests using a Physical Skin Model (Agarose Hydrogel Model)*: The dissolution of the drug-loaded MNs was evaluated using an agarose hydrogel (1.4% w/v) that mimicked the skin's dynamic viscoelastic properties.[40,47] The hydrogel was covered with a layer of food-grade adherent plastic wrap (thickness of $14 \pm 1$ µm, $n = 30$, measured with a handheld digital micrometer (Mitutoyo Corporation, Tokyo, Japan)) to simulate the resistance encountered by the MNs when in contact with the *stratum corneum*. The MN was inserted into the skin simulant using a spring applicator (Micropoint Technologies Pte Ltd., Singapore) and photographed at determined time points. Additionally, the MN patches ($n = 9$) were inserted in the skin model, as described above, and retrieved at fixed time points to gauge the amount of drug retained. Each patch was dissolved in a vial containing 10 mL of PBS at 37 °C, and the DCF content in each aliquot was determined by UV-vis ($y = 16.068x - 0.0013$; $R^2 = 0.9999$, 0.001–0.02 mg $mL^{-1}$ DCF). The amount of diclofenac retained in the patches was calculated following Equation (2), where $m_{DCF}$ is the mass of drug retained in the patch and $m_{CMC\_DCF}$ is the mass of the patch before insertion

$$\text{DCF retained } [\%] = [(m_{DCF})/(m_{CMC\_DCF})] \times 100 \tag{2}$$

*In Vitro Cytotoxicity Assay*: The cytotoxicity of the MN arrays was evaluated in HaCaT cells using the MTT assay.[48] The cells were grown in complete DMEM supplemented with 10% FBS, $2 \times 10^{-3}$ M L-glutamine, 10 000 U $mL^{-1}$ penicillin/streptomycin, and 250 µg $mL^{-1}$ fungizone at 37 °C with 5% $CO_2$ humidified atmosphere and observed daily in an Eclipse T100 microscope (Nikon, Tokyo, Japan). Each MN array was sterilized by UV radiation, incubated with complete DMEM medium at 37 °C, 5% $CO_2$, for 24 h, and then diluted 20 times with DMEM medium to obtain the test samples. HaCaT cells cultured in full DMEM media served as a negative control. HaCaT cells were seeded in 96 wells plates, at 6000 cells $well^{-1}$, and incubated with culture medium for 24 h for adhesion. Subsequently, the culture medium was replaced with 100 µL of the CMC MNs and CMC_DCF MNs samples and incubated for 24 h. At the end of incubation, 50 µL of MTT (1 g $L^{-1}$) was added to each well and incubated for 4 h at 37 °C in a 5% $CO_2$ humidified atmosphere. The culture medium with MTT was then removed and replaced with 150 µL of DMSO. The plate was placed in a shaker for 2 h in the dark to dissolve the formazan crystals completely. The absorbance of the samples was measured with a BioTek Synergy HT plate reader (Synergy HT Multi-Mode, BioTek, Winooski, VT) at 570 nm with blank corrections. The cell viability was calculated with respect to the control cells according to Equation (3), where $Abs_{sample}$ is the

absorbance of the sample, $Abs_{DMSO}$ is the absorbance of the DMSO, and $Abs_{control}$ is the absorbance of the control.

$$Cell\ viability\ [\%] = \left[\frac{Abs_{sample} - Abs_{DMSO}}{Abs_{control} - Abs_{DMSO}}\right] \times 100 \qquad (3)$$

*Statistical Analysis*: All results were presented as mean values ± standard deviation ($n \geq 3$). For the in vitro assays, Anderson–Darling, D'Agostino–Pearson, and Shapiro–Wilk tests were used to determine the normality of the data distribution. Analysis of variance (ANOVA), followed by Tukey's or Dunnett's tests, was employed to determine the statistical significance of the data established at $p < 0.05$ (GraphPad Prism, version 8.0.2, GraphPad Software Inc., San Diego, CA, USA).

## Acknowledgements

## Conflict of Interest

The authors declare no conflict of interest.

## Author Contributions

A.C.Q.S.: Investigation, Methodology, Writing—original draft, Writing—review & editing; B.P.: Investigation, Methodology, Writing—review & editing; N.S.L.: Methodology, Writing—review & editing; P.C.C.: Methodology, Resources, Writing—review & editing; I.F.A.: Methodology, Resources, Writing—review & editing; P.D.-P.: Resources, Writing—review & editing; I.C.-S.: Investigation, Resources, Writing—review & editing; H.O.: Methodology, Resources, Writing—review & editing; C.V.: Methodology, Supervision, Writing—review & editing; A.J.D.S.: Methodology, Supervision, Writing—review & editing; C.S.R.F.: Conceptualization, Funding acquisition, Methodology, Resources, Supervision, Writing—review & editing.

## Data Availability Statement

All data are included in the manuscript in the form of tables and graphics.

## Keywords

[1] D. R. Axon, M. J. Patel, J. R. Martin, M. K. Slack, *Scand. J. Pain* **2019**, *19*, 9.
[2] D. H. Cisewski, S. M. Motov, *Turk. J. Emerg. Med.* **2019**, *19*, 1.
[3] S. Calatayud, J. V. Esplugues, in *NSAIDs and Aspirin* (Ed: A. Lanas), Springer International Publishing, Cham, Switzerland, **2016**, pp. 3.
[4] D. M. McCarthy, in *NSAIDs and Aspirin* (Ed: A. Lanas), Springer International Publishing, Cham, Switzerland, **2016**, pp. 123.
[5] C. Baigent, N. Bhala, J. Emberson, A. Merhi, S. Abramson, N. Arber, J. A. Baron, C. Bombardier, C. Cannon, M. E. Farkouh, G. A. FitzGerald, P. Goss, H. Halls, E. Hawk, C. Hawkey, C. Hennekens, M. Hochberg, L. E. Holland, P. M. Kearney, L. Laine, A. Lanas, P. Lance, A. Laupacis, J. Oates, C. Patrono, T. J. Schnitzer, S. Solomon, P. Tugwell, K. Wilson, J. Wittes, et al., *Lancet* **2013**, *382*, 769.
[6] K. Y. Ho, K. A. Gwee, Y. K. Cheng, K. H. Yoon, H. T. Hee, A. R. Omar, *J. Pain Res.* **2018**, *11*, 1937.
[7] F. Sabbagh, B. S. Kim, *J. Controlled Release* **2022**, *341*, 132.
[8] MedlinePlus, Diclofenac Transdermal Patch, https://medlineplus.gov/druginfo/meds/a611001.html (accessed: October 2022).
[9] MedlinePlus, Diclofenac Topical (arthritis pain), https://medlineplus.gov/druginfo/meds/a611002.html (accessed: October 2022).
[10] B. R. Da Costa, S. Reichenbach, N. Keller, L. Nartey, S. Wandel, P. Jüni, S. Trelle, *Lancet* **2017**, *390*, e21.
[11] C. Zeng, J. Wei, M. S. M. Persson, A. Sarmanova, M. Doherty, D. Xie, Y. Wang, X. Li, J. Li, H. Long, G. Lei, W. Zhang, *Br. J. Sports Med.* **2018**, *52*, 642.
[12] F. Bariguian Revel, M. Fayet, M. Hagen, *Rheumatol. Ther.* **2020**, *7*, 217.
[13] D. F. S. Fonseca, C. Vilela, A. J. D. Silvestre, C. S. R. Freire, *Int. J. Biol. Macromol.* **2019**, *136*, 704.
[14] V. Alimardani, S. S. Abolmaali, G. Yousefi, Z. Rahiminezhad, M. Abedi, A. Tamaddon, S. Ahadian, *J. Clin. Med.* **2021**, *10*, 181.
[15] T. Waghule, G. Singhvi, S. K. Dubey, M. M. Pandey, G. Gupta, M. Singh, K. Dua, *Biomed. Pharmacother.* **2019**, *109*, 1249.
[16] D. F. S. Fonseca, P. C. Costa, I. F. Almeida, P. Dias-Pereira, I. Correia-Sá, V. Bastos, H. Oliveira, M. Duarte-Araújo, M. Morato, C. Vilela, A. J. D. Silvestre, C. S. R. Freire, *Carbohydr. Polym.* **2020**, *241*, 116314.
[17] M.-C. Chen, M.-H. Ling, K.-Y. Lai, E. Pramudityo, *Biomacromolecules* **2012**, *13*, 4022.
[18] D. F. S. Fonseca, C. Vilela, R. J. B. Pinto, V. Bastos, H. Oliveira, J. Catarino, P. Faísca, C. Rosado, A. J. D. Silvestre, C. S. R. Freire, *Mater. Sci. Eng., C* **2021**, *118*, 111350.
[19] M.d. S. Rahman, M.d. S. Hasan, A. S. Nitai, S. Nam, A. K. Karmakar, M.d. S. Ahsan, M. J. A. Shiddiky, M. B. Ahmed, *Polymers* **2021**, *13*, 1345.
[20] S. Javanbakht, A. Shaabani, *Int. J. Biol. Macromol.* **2019**, *133*, 21.
[21] J. W. Lee, J.-H. Park, M. R. Prausnitz, *Biomaterials* **2008**, *29*, 2113.
[22] G. Bonfante, H. Lee, L. Bao, J. Park, N. Takama, B. Kim, *Micro Nano Syst. Lett.* **2020**, *8*, 13.
[23] B.-M. Lee, C. Lee, S. F. Lahiji, U.-W. Jung, G. Chung, H. Jung, *Pharmaceutics* **2020**, *12*, 366.
[24] J. D. Kim, M. Kim, H. Yang, K. Lee, H. Jung, *J. Controlled Release* **2013**, *170*, 430.
[25] M. R. Zare, M. Khorram, S. Barzegar, B. Sarkari, Q. Asgari, S. Ahadian, K. Zomorodian, *Int. J. Biol. Macromol.* **2021**, *182*, 1310.
[26] L. Yan, A. P. Raphael, X. Zhu, B. Wang, W. Chen, T. Tang, Y. Deng, H. J. Sant, G. Zhu, K. W. Choy, B. K. Gale, T. W. Prow, X. Chen, *Adv. Healthcare Mater.* **2014**, *3*, 555.
[27] I.-C. Lee, W.-M. Lin, J.-C. Shu, S.-W. Tsai, C.-H. Chen, M.-T. Tsai, *J. Biomed. Mater. Res., Part A* **2017**, *105*, 84.
[28] J.-W. So, H.-H. Park, S. S. Lee, D.-C. Kim, S.-C. Shin, C.-W. Cho, *Drug Delivery* **2009**, *16*, 52.
[29] T. Ilić, S. Savić, B. Batinić, B. Marković, M. Schmidberger, D. Lunter, M. Savić, S. Savić, *Eur. J. Pharm. Sci.* **2018**, *125*, 110.
[30] S. R. Vučen, G. Vuleta, A. M. Crean, A. C. Moore, N. Ignjatović, D. Uskoković, *J. Pharm. Pharmacol.* **2013**, *65*, 1451.

ADVANCED
SCIENCE NEWS

www.advancedsciencenews.com

[M] acro-molecular
Bioscience

www.mbs-journal.de

[31] M. T. C. Mccrudden, A. Z. Alkilani, C. M. Mccrudden, E. Mcalister, H. O. Mccarthy, A. D. Woolfson, R. F. Donnelly, *J. Controlled Release* **2014**, *180*, 71.

[32] K. Yu, X. Yu, S. Cao, Y. Wang, Y. Zhai, F. Yang, X. Yang, Y.i Lu, C. Wu, Y. Xu, *Acta Pharm. Sin. B* **2021**, *11*, 505.

[33] GlaxoSmithKline, Voltaren Diclofenac gel 1%, https://www.voltaren gel.com/living-with-arthritis/managing-arthritis/over-the-counter-diclofenac-gel/ (accessed: October 2022).

[34] N. H. C. S. Silva, A. F. Rodrigues, I. F. Almeida, P. C. Costa, C. Rosado, C. P. Neto, A. J. D. Silvestre, C. S. R. Freire, *Carbohydr. Polym.* **2014**, *106*, 264.

[35] D. S. Lakshmi, N. Trivedi, C. R. K. Reddy, *Carbohydr. Polym.* **2017**, *157*, 1604.

[36] D. R. Biswal, R. P. Singh, *Carbohydr. Polym.* **2004**, *57*, 379.

[37] L. Song, F. Liu, C. Zhu, A. Li, *Chem. Eng. J.* **2019**, *369*, 641.

[38] C. Rosca, M. I. Popa, G. Lisa, G. C. Chitanu, *Carbohydr. Polym.* **2005**, *62*, 35.

[39] M. Bartolomei, P. Bertocchi, E. Antoniella, A. Rodomonte, *J. Pharm. Biomed. Anal.* **2006**, *40*, 1105.

[40] J. P. F. Carvalho, A. C. Q. Silva, V. Bastos, H. Oliveira, R. J. B. Pinto, A. J. D. Silvestre, C. Vilela, C. S. R. Freire, *Nanomaterials* **2020**, *10*, 628.

[41] W. Li, B. Sun, P. Wu, *Carbohydr. Polym.* **2009**, *78*, 454.

[42] A. Pettignano, A. Charlot, E. Fleury, *Polymers* **2019**, *11*, 1227.

[43] J.-H. Park, M. G. Allen, M. R. Prausnitz, *J. Controlled Release* **2005**, *104*, 51.

[44] E. Larrañeta, J. Moore, E. M. Vicente-Pérez, P. González-Vázquez, R. Lutton, A. D. Woolfson, R. F. Donnelly, *Int. J. Pharm.* **2014**, *472*, 65.

[45] L. K. Vora, A. J. Courtenay, I. A. Tekko, E. Larrañeta, R. F. Donnelly, *Int. J. Biol. Macromol.* **2020**, *146*, 290.

[46] M. A. Momoh, F. C. Kenechukwu, M. O. Adedokun, C. E. Odo, A. A. Attama, *Drug Delivery* **2014**, *21*, 193.

[47] A. K. Dąbrowska, G.-M. Rotaru, S. Derler, F. Spano, M. Camenzind, S. Annaheim, R. Stämpfli, M. Schmid, R. M. Rossi, *Skin Res. Technol.* **2016**, *22*, 3.

[48] H. M. N. Iqbal, T. Keshavarz, in *Biomedical Composites* (Ed: L. Ambrosio), Elsevier, New York **2017**, pp. 303–334.

[49] A. Bhattacharjee, J. A. Lopes-Da-Silva, M. G. Freire, J. A. P. Coutinho, P. J. Carvalho, *Fluid Phase Equilib.* **2015**, *400*, 103.